Since January 2020 Elsevier has created a COVID-19 resource centre with free information in English and Mandarin on the novel coronavirus COVID-19. The COVID-19 resource centre is hosted on Elsevier Connect, the company's public news and information website.

Computers in Biology and Medicine 134 (2021) 104524

Contents lists available at ScienceDirect

Computers in Biology and Medicine

journal homepage: www.elsevier.com/locate/compbiomed

Screening of natural compounds from *Cyperus rotundus* Linn against SARS-CoV-2 main protease (M^{pro}): An integrated computational approach

S. Birendra Kumar [a], Swati Krishna [a], Sneha Pradeep [a], Divya Elsa Mathews [a], Ramya Pattabiraman [a], Manikanta Murahari [b,**], T.P. Krishna Murthy [a,*]

[a] Department of Biotechnology, M. S. Ramaiah Institute of Technology, Bengaluru, 560054, Karnataka, India
[b] Department of Pharmaceutical Chemistry, Faculty of Pharmacy, M. S. Ramaiah University of Applied Sciences, Bengaluru, 560054, Karnataka, India

ARTICLE INFO

Keywords:
Main protease (M^{pro})
Cyperus rotundus Linn
β-amyrin
Stigmasta-5,22-dien-3-ol
Molecular docking and molecular dynamics simulation

ABSTRACT

Coronavirus disease 2019 (COVID-19) is a viral respiratory disease that has been spreading across the globe. The World Health Organization (WHO) declared it as a public health emergency. The treatment of COVID-19 has been hampered due to the lack of effective therapeutic efforts. Main Protease (M^{pro}) is a key enzyme in the viral replication cycle and its non-specificity to human protease makes it a potential drug target. *Cyperus rotundus* Linn, which belongs to the *Cyperaceae* family, is a traditional herbal medicine that has been widely studied for its antiviral properties. In this study, a computational approach was used to screen natural compounds from *C. rotundus* Linn using BIOVIA Discovery Suite and novel potential molecules against M^{pro} of SARS-CoV-2 were predicted. Molecular docking was performed using LibDock protocol and selected ligands were further subjected to docking analysis by CDOCKER. The docking scores of the selected ligands were compared with standard antiretroviral drugs such as lopinavir and ritonavir to assess their binding potentials. Interaction pharmacophore analysis was then performed for the compounds exhibiting good binding scores to evaluate their protein–ligand interactions. The selected protein–ligand complexes were subjected to molecular dynamics simulation for 50 ns. Results of binding free energy analysis revealed that two compounds—β-amyrin and stigmasta-5,22-dien-3-ol—exhibited the best binding interactions and stability. Finally, absorption, distribution, metabolism, excretion, and toxicity (ADMET) studies were performed to understand the pharmacokinetic properties and safety profile of the compounds. The overall results indicate that the phytochemicals from *Cyperus rotundus* Linn, namely β-amyrin and stigmasta-5,22-dien-3-ol, can be screened as potential inhibitors of SARS-CoV-2 M^{pro}.

1. Introduction

The globally-spread pandemic caused by novel coronavirus SARS-CoV-2 (COVID-19) affects various species ranging from animals to humans, causing serious forms of respiratory diseases [1]. Evidence suggests that COVID-19 emerged in Wuhan, Hubei province (China), where it caused the main cluster of atypical pneumonia. It is supposed to have originated from bats and pangolins and now, the disease is spreading rapidly through humans [2]. Until now (April 19, 2021), on a world scale, COVID-19 has affected close to 141 million people and has caused more than 3.01 million deaths approximately. In the current upsurge, it is necessary to identify the causal agent for diagnosing the disease and developing control measures [3].

SARS-CoV-2 is a large enveloped virus with spike glycoproteins on its outer surface and a nucleocapsid protein containing a positive sense single-stranded ribonucleic acid (ssRNA). It has a high frequency of mutation and recombination [4]. The mechanism used by the virus for entry into host cells involves binding to the angiotensin-converting enzyme 2 (ACE2) receptors of human cells [5]. Once the coronavirus attaches to the host cell, it has a clear path to invade the cells even before the immune system can realize that the body has been affected by an external virus. The virus encodes main protease (M^{pro}), papain-like protease (PL^{pro}), spike protein (S), RNA-dependent RNA polymerase (RdRp/nsp12), and NTPase/helicase (nsp13), all of which are potential antiviral drug targets. These entities are responsible for the cleavage of polyproteins and formation of active substances for replication of the virus inside the host cell. However, in contrast to other proteins encoded by the virus, M^{pro} exhibits unique substrate specificity towards viral

* Corresponding author.
** Corresponding author.
E-mail addresses: manikanta.murahari@gmail.com, manikanta.py.ph@msruas.ac.in (M. Murahari), tpk@live.in, krishnamurthytp@msrit.edu (T.P.K. Murthy).

https://doi.org/10.1016/j.compbiomed.2021.104524
Received 6 February 2021; Received in revised form 22 May 2021; Accepted 22 May 2021
Available online 29 May 2021

polypeptide sequences, making it an attractive and ideal choice as a drug target. Viral proteases have been studied thoroughly as drug targets and studies have led to the identification of various approved drugs. The key enzyme in viral replication is M^{pro}, also called as 3-chymotrypsin-like protease ($3CL^{pro}$). M^{pro} is a cysteine protease with an active site comprising a catalytic dyad (cysteine and histidine). It is responsible for proteolytic processing and undergoes maturation by auto cleaving into dimeric active conformation [6]. Since M^{pro} does not demonstrate any similarity and specificity to human host cell protease, its inhibition can halt the production of infectious viral particles and thus reduce symptoms of the disease [7].

Globally, to date, there are 6 clinically-accepted vaccines against coronavirus. These include Pfizer-BioNTech, Moderna, Johnson & Johnson/Janssen, Sputnik V, Covaxin and Covishield [8–10]. Drugs such as remdesivir, chloroquine or hydroxychloroquine and lopinavir (for hospitalised patients only) have been repurposed to combat SARS-CoV-2. Among these, remdesivir has been approved by the United States Food and Drug Administration (FDA) for COVID-19 treatment [11]. However, the public is reluctant to use these medicines due to their limited availability in comparison to the affected population, lack of clear knowledge about their efficacy rate and side effects. Hence, it is crucial to develop novel and effective antiviral drugs to combat diseases such as COVID-19. Due to the proven studies on medicinal plants as sources of antiviral agents, it is advantageous to explore their potential towards the development of treatment for COVID-19.

Cyperus rotundus Linn belongs to the Cyperaceae family and is also known as purple nutsedge or nutgrass. It is a traditional herbal medicine widely used as an analgesic, sedative, antispasmodic and antimalarial, and has been used to treat gastrointestinal disorders and to relieve diarrhoea. Although *C. rotundus* is indigenous to India, it is also found in other geographical locations such as tropical, subtropical and temperate regions. The tubers are used in Ayurvedic medicine and the herb has been mentioned in ancient texts for the treatment of various chronic ailments [12]. Phytochemical studies have shown that this herb contains essential oils, flavonoids, terpenoids, mono- and sesquiterpenes. These biologically-active phytochemicals have pharmacological properties that have been proven to be safe and effective in the treatment of chronic disorders [13]. The essential oils of this herb have been tested for their antiviral activity against hepatitis A, herpes simplex type 1, and coxsackie viruses. A report on the modulation of CYP3A4 enzyme by the rhizome fractions of C. *rotundus* suggests its safe consumption concerning drug metabolism and efficacy. The study also provided the basis for the hepatoprotective and hepatitis B virus (HBV) inhibitory activity of *C. rotundus* [14]. In the present study, a virtual screening of the biologically-active compounds identified in *C. rotundus* Linn was carried out to predict the best inhibitors against SARS-CoV-2 main protease.

2. Materials and methods

2.1. Phytochemicals database

A library of 389 phytochemical constituents of *C. rotundus* was designed through a comprehensive literature survey as given in Supplementary Table S1. The three-dimensional (3D) structures of ligands were obtained from the PubChem (https://pubchem.ncbi.nlm.nih.gov/) database. The structures that were not available in PubChem were drawn using MarvinSketch (https://chemaxon.com/products/marvin) [15].

2.2. Drug-like properties

Physicochemical characteristics of the 389 phytochemicals of *C. rotundus* were analyzed by Lipinski's Rule of Five (RO5) and Veber's Rule, the preliminary rules to be satisfied for drug-likeness. RO5 dictates that a small molecule or drug shows good oral bioavailability, smooth membrane permeability and strong gastrointestinal absorption in the human intestine when it satisfies the following criteria: logP $\leq$5; molecular weight $\leq$500 Da; hydrogen bond acceptors $\leq$10 and hydrogen bond donors $\leq$5 [16,17]. In Veber's Rule, the main factor influencing drug absorption in the lumen is the number of rotatable bonds, which in turn indicates the molecular flexibility, bioavailability and binding potency of the drug. The criteria followed by this rule include rotatable bonds $\leq$10 and total number of hydrogen bond donors and acceptors $\leq$12. A polar surface area limit of less than 140 $Å^2$ is also a filtering criterion [17–19]. The compounds that satisfied both the rules, with violation of at most one criterion, were selected for further analysis.

2.3. Ligand preparation

The selected ligands were refined using the "Prepare Ligand" module of receptor–ligand interaction tool in Discovery Studio (DS 2020) (Accelrys, San Diego, USA) by removing duplicates, enumerating isomers and tautomers and generating 3D conformations. A conformational search was applied to all the ligands and the best conformers underwent energy minimization using the CHARMM (Chemistry at HARvard Macromolecular Mechanics) force field [20,21].

2.4. Protein selection and preparation

The crystal structure of SARS-CoV-2 M^{pro} (PDB ID: 6LU7) was retrieved from the Protein Data Bank (PDB). The protein was refined using the "Prepare Protein" module of receptor–ligand interaction tool in DS 2020 [20]. The protein preparation was carried out by first removing the native ligand followed by correcting the ionization and tautomeric states of amino acid residues by adding hydrogen atoms to the protein. The missing loops and atoms were modelled and alternate conformations were removed for further refinement of the crystallographic structure. Furthermore, to generate a stable conformation, the protein was subjected to energy minimization by applying the CHARMM force field using the steepest descent algorithm [22].

2.5. Molecular docking and calculations of binding energy

Molecular docking was performed to analyze the binding affinity and nature of the interaction between selected ligands and the protein (M^{Pro}). LibDock module, available in DS 2020, was employed for docking. In essence, the LibDock protocol structurally rearranges the ligand in response to the receptor to generate docked poses [23]. A receptor-grid box with the attributes X = −10.79, Y = 12.54 and Z = 68.91 was adopted and the bioactive conformations were simulated. The ligands exhibiting a LibDock score greater than 100 were filtered and were further analyzed using the CDOCKER (CHARMM-based DOCKER) protocol. The top-ranked poses with the most negative, favourable interactions were carried forward for further analysis [24]. Finally, the "Calculate Binding Energy" module of CDOCKER was used to calculate the binding energy of filtered poses. The calculations were done based on implicit solvation using the molecular mechanics-generalized Born with molecular volume (MM/GBMV), molecular mechanics Poisson–Boltzmann surface area (MM/PBSA) and total binding energy model [25].

2.6. Interaction pharmacophore generation

To evaluate the interactions between the protein and ligands filtered from binding energy calculation studies, the amino acid residue contributions and nature of interactions were examined. Further, receptor–ligand pharmacophores was generated for the compounds using DS 2020. Essentially, in interaction pharmacophore generation, a set of pharmacophore models are generated based on features that correspond to receptor–ligand interaction. Ligand features such as hydrogen bond acceptor, hydrogen bond donor, hydrophobic features, negative ionizable features and presence of aromatic rings are considered and

analyzed [26] to gain further insights into the nature of functional groups in the ligand.

2.7. Molecular dynamics simulations and binding free energy analysis

The complex structure of M^{pro} with selected ligands identified from docking analysis, binding free energy calculations, molecular interaction studies and interaction pharmacophore analyses were carried out. The molecular dynamics simulation (MD) was done using GROMACS version 2019.4 [27]. The system preparation was done following previously-published papers [28–30]. The ligand topology was generated from PRODRG web server [31] and the protein parameters were generated using gromos54a7 force field. The systems thus prepared were first vacuum-minimized for 1500 steps using the steepest descent algorithm. The structures were then solvated in a cubic periodic box with a water extended simple point charge (SPCE) model. The complex systems were further maintained in an appropriate environment having a salt concentration of 0.15 M. The system was electro neutralized by adding an appropriate concentration of sodium (Na^+) and chlorine (Cl^-) counter ions. Subsequently, energy minimization was carried out for 50, 000 steps. The next step was equilibration, which was performed in two steps. The first step consisted of constant volume (NVT) equilibration and the other was constant pressure (NPT) equilibration. Each resultant structure from the NPT equilibration phase was subjected to a final production run in the NPT ensemble for a simulation time of 50 ns.

Root mean square deviation (RMSD) and root mean square fluctuation (RMSF) of the protein were calculated using gmx rms and gmx rmsf tools respectively [32]. The gmx gyrate and gmx sasa tools were used to calculate the radius of gyration (Rg) and solvent accessible surface area (SASA) respectively. The MM/PBSA approach was employed to understand the binding free energy (ΔG binding) of an inhibitor with protein over the simulation time. The GROMACS utility g_mmpbsa was employed to estimate the binding free energy [33]. To obtain an accurate result, we computed ΔG for the last 20 ns with dt 1000 frames [16].

2.8. Prediction of ADMET and biological activity

The hit molecules identified were subjected to ADMET prediction studies. The pkCSM [34] tool was used to predict the pharmacokinetic properties wherein various sub-criteria related to absorption (A), distribution (D), metabolism (M), excretion (E), and toxicity (T) were analyzed to classify the ligand as a potential drug molecule. Further, to predict the biological activity of the hit compounds, PASS (prediction of activity spectra for substances) (http://www.pharmaexpert.ru/passonline/index.php) software was employed.

3. Results and discussion

A critically-evaluated library containing 389 ligands was derived from *C. rotundus* through a thorough literature survey. These compounds were then filtered for drug-relevant properties based on Lipinski's Rule of 5 and Veber's rule. This resulted in 354 relevant ligands, which were subjected to the ligand preparation module of DS 2020, generating a total of 440 ligands.

3.1. Docking studies

The molecular docking technique is a structure-based drug design approach to understand the essential amino acid interactions between the selected protein and generated ligands and the stability associated with conformational changes [35]. The 440 ligands obtained after ligand preparation and filtration steps were subjected to docking at the active site of M^{pro} using LibDock protocol available in DS 2020. The LibDock protocol generated a total of 7938 conformers. The scoring function and binding interaction for every conformational receptor–ligand complex pose were chosen as selection criteria [36]. The ligands that showed a LibDock score greater than 100 were taken for further analysis by CDOCKER. The flexible CDOCKER method is an extension of the family of complete docking solutions available within CHARMM [37]. A total of 30 ligands were selected using the LibDock protocol using the above-mentioned criteria. The LibDock score and molecular structure of the top 30 compounds are presented in Table 1 and Supplementary Table S2 respectively.

Further, all 30 ligands were docked into the defined binding site of M^{pro} using the CDOCKER algorithm, generating a total of 300 different poses of the 12 compounds (shown in Table 2). The parameters CDOCKER energy and CDOCKER binding interaction energy were evaluated to identify the best inhibitors. CDOCKER energy is expressed in terms of combined energy produced by the sum of internal ligand strain energy and receptor–ligand interaction energy. The values of these two parameters indicate the strength of interaction between the protein and ligands [38]. Compounds that exhibited negative binding energy were taken forward for further analysis, accounting for a total of 12 ligands as shown in Table 2. The class, property and toxicity of the top 12 compounds are given in Supplementary Table S3.

3.2. Binding free energy calculation

The most popular methods for binding free energy calculation are MM/PBSA and MM/GBMV due to their accuracy in comparison to most scoring functions of molecular docking [39]. MM/PBSA and molecular mechanics-generalized Born surface area (MM/GBSA) calculations were carried out for the 12 ligands using the "Calculate Binding Energy" protocol of DS 2020, as shown in Table 3.

3.3. Molecular interaction studies

The docking results were visualized with the help of DS 2020 for evaluation of receptor–ligand interactions. The best binding postures of protein–ligand communication are depicted in Fig. 1 and tabulated in Table 2. Lupeol displayed the best docking affinity to M^{pro}, as seen by the CDOCKER score of −70.03 kcal/mol followed by β-amyrin acetate with

Table 1
LibDock score of the selected 30 compounds.

Sl. No.	Ligand Name	LibDock Score
1.	(E,E)-farnesol	100.56
2.	[4−] hydroxy cinnamic acid	118.97
3.	3,4-seco-mansumbinoic acid	106.42
4.	Adenosine	105.45
5.	Ammiol	100.29
6.	Aureusidin	117.92
7.	β-amyrin	113.58
8.	β-amyrin acetate	101.08
9.	β-sitosterol	133.29
10.	Cyperusol B1	101.59
11.	Allagic_acid	111.02
12.	Isoliquiritigenin	112.64
13.	Isorhamnetin	126.88
14.	Kaempferol	119.05
15.	Lupeol	104.49
16.	Luteolin	115.30
17.	Luteolin_3-methyl_ether	128.67
18.	Luteolin_5,_3-dimethyl_ether	133.94
19.	Luteolin_5-methyl_ether	131.71
20.	oleanolic_acid	106.06
21.	Piceid	150.22
22.	Pinoquercetin	122.50
23.	Quercetin	129.08
24.	Rosenonolactone	101.12
25.	Scaberin	119.86
26.	Stigmasta-5,22-dien-3-ol	128.51
27.	sugetriol_triacetate	102.50
28.	Sugetriol-3,9-diacetate	106.47
29.	Uridine	110.97
30.	Valerenyl_acetate	105.77

Table 2
CDOCKER scores and molecular interactions of 12 ligands.

Sl. No.	Ligand Name	CDOCKER energy (kcal/mol)	Molecular interactions with distance (Å)
1	Sugetriol-3,9-diacetate	−39.56	**H-Bonds**: HIS 41 (4.44); MET 165 (5.73); GLN 189 (4.57); **Hydrophobic Bonds:** CYS 145 (3.64); MET 165 (4.88); HIS 163 (5.80)
2	Adenosine	−5.93	**H-Bonds**: ASN 142 (4.67); PHE 140 (5.20); GLU 166 (4.25); **Hydrophobic Bonds:** CYS 145 (5.41) **Unfavorable Donor-Donor:** HIS 163 (5.44)
3	β-Sitosterol	−40.53	**Hydrophobic Bonds:** HIS 41 (5.55); CYS 145 (5.13, 5.42); PRO 168 (4.94)
4	β-Amyrin acetate	−59.33	**Hydrophobic Bonds:** HIS 41 (7.19); CYS 145 (6.71); PRO 168 (4.69, 6.02)
5	Stigmasta-5,22-dien-3-ol	−45.18	**H-Bonds**: THR 26 (4.40) **Hydrophobic Bonds:** HIS 41 (5.26); CYS 145 (4.65, 5.28); MET 165 (4.84); PRO 168 (4.41)
6	β-Amyrin	−48.36	**H-Bonds**: CYS 145 (4.90); **Hydrophobic Bonds:** HIS 41 (7.70); CYS 145 (5.57, 6.49); PRO 168 (4.23, 5.38, 6.62)
7	Lupeol	−70.04	**Hydrophobic Bonds:** HIS 41 (7.02); MET 49 (6.59); CYS 145 (4.58, 6.92)
8	(E,E)-Farnesol	−38.95	**H-Bonds**: GLU 166 (4.90); PRO 168 (5.02); THR 190 (4.73); **Hydrophobic Bonds:** CYS 145 (4.13); MET 165 (5.58)
9	Oleanolic acid	−58.75	**H-Bonds**: PRO 168 (3.97); **Hydrophobic Bonds:** HIS 41 (7.16); CYS 145 (5.48, 6.59); PRO 168 (4.67, 6.31)
10	Valerenyl acetate	−44.81	**Hydrophobic Bonds:** HIS 41 (5.89); MET 49 (5.64, 6.36); HIS 163 (5.63); MET 165 (4.27, 4.40); **Electrostatic Bonds:** GLU 166 (4.19)
11	Cyperusol B1	−22.17	**H-Bonds**: HIS 41 (4.83); HIS 164 (5.30); **Hydrophobic Bonds:** HIS 41 (4.08, 6.88); MET 49 (4.39); CYS 145 (6.44)
12	Rosenonolactone	17.54	**H-Bonds**: ASN 142 (3.57, 4.48); **Hydrophobic Bonds:** CYS 145 (4.93); HIS 163 (5.66)
13	Lopinavir	−50.25	**H-Bonds:** PHE 140 (2.56); LEU 141 (2.76); ASN 142 (3.02); GLU 166 (2.54); GLN 189 (1.93); MET 165 (2.34) **Hydrophobic Bonds:** MET 49 (4.84); MET 165 (3.68); CYS 145 (5.97)
14	Ritonavir	−68.58	**H-Bonds:** ASN 142 (3.10); CYS 145 (2.45); GLU 166 (2.38); GLN 189 (2.89); MET 165 (3.01) **Hydrophobic Bonds:** MET 49 (4.58); PRO 168 (2.87)

a docking score of −59.33 kcal/mol. The compounds oleanolic acid, β-amyrin, stigmasta-5,22-dien-3-ol and valrenyl acetate displayed good binding affinity to M^{pro} with CDOCKER scores of −58.76 kcal/mol, −48.36 kcal/mol, 45.12 kcal/mol, and −44.81 kcal/mol respectively. Following these, the compounds β-sitosterol, sugetriol-3,9-diacetate, (E,E)-farnesol, cyperusol B1 and adenosine demonstrated moderate to low binding potential to M^{pro} with docking scores of −40.53 kcal/mol, −39.56 kcal/mol, −38.95 kcal/mol, −22.17 kcal/mol, and −5.93 kcal/mol respectively. The compound rosenonolactone had a positive CDOCKER score of 17.54 kcal/mol, suggesting unfavorable binding.

Table 3
MM-PBSA, MM-GBMV and Total Binding Energy values for the 12 ligands.

Ligand Name	Binding Energy (kcal/mol)		
	MM/PBSA	MM-GBMV	Total Binding Energy
β-Amyrin	−7.67	−14.09	−40.29
β-Sitosterol	−7.26	−10.60	−47.84
Valerenyl Acetate	−6.77	−13.75	−27.22
(E,E)-Farnesol	−6.76	−11.04	−36.96
Lupeol	−3.83	−11.28	−38.67
Sugetriol-3,9-diacetate	−3.50	−11.09	−93.00
Rosenonolactone	−3.21	−9.38	−8.74
Cyperusol B1	−1.68	−5.86	−10.58
Stigmasta-5,22-dien-3-ol	−0.38	−9.17	−44.52
Oleanolic acid	1.35	−11.43	−35.99
β-Amyrin acetate	2.17	−13.09	−47.68
Adenosine	4.63	−8.07	−63.46

The docking studies were also carried out with existing antiretroviral protease inhibitors, namely lopinavir and ritonavir. Their CDOCKER scores were compared with the twelve identified phytochemicals. Lopinavir exhibited a binding energy score of −50.25 kcal/mol whereas ritonavir exhibited a score of −68.58 kcal/mol. Lupeol had better binding energy than both the commercially-available antiretrovirals. The compounds β-amyrin acetate, oleanolic acid, β-amyrin, and stigmasta-5,22-dien-3-ol also exhibited binding energies that were comparable with those of standard drugs.

Further analysis revealed that all the phytoconstituents interacted moderately at the active site of M^{pro}, thereby suggesting their probable inhibitory tendencies against SARS-CoV-2 M^{pro}. On observing the non-covalent interactions of phytochemicals with M^{pro}, it was seen that the ligands interacted with either both or at least one catalytic residue, i.e. Cys145 and His41, detected by CDOCKER (shown in Table 2 and Fig. 1). The interaction of β-amyrin with M^{pro} was stabilized by one hydrogen bond involving Cys145 residue and 6 hydrophobic interactions involving Pro168, His41, and Cys145 residues. Oleanolic acid interacted with M^{pro} via Pro168 (involved in both hydrogen bonding and hydrophobic interactions), His41, and Cys145 residues. Both hydrogen bonds and hydrophobic interactions were responsible for the stability of the stigmasta-5,22-dien-3-ol–M^{pro} complex. Thr26 contributed towards hydrogen bonding while His41, Cys145, Pro168, and Met165 were involved in hydrophobic interactions. For the valrenyl acetate–M^{pro} complex, interaction stability was achieved by His41, Met49, His163, and Met165 residues, contributing to the hydrophobic bond; the Glu166 residue was involved in the electrostatic bond. Overall, these ligands exhibited hydrogen bonding and hydrophobic interactions with catalytic residues Cys145 and His41. In the case of β-sitosterol and β-amyrin acetate, the hydrophobic bonds formed by His41, Cys145, and Pro168 stabilized their binding to M^{pro}. The hydrogen bonds formed by His4, Met165, and Gln189 and the hydrophobic interactions formed by Cys145, Met165, and His163 conferred stability to the sugetriol-3,9-diacetate–M^{pro} complex. The Lupeol–M^{pro} complex gained stability through the hydrophobic bonds contributed by His41, Cys145, and Met49 residues. The hydrophobic bonds formed with Cys145 and Met165 as well as hydrogen bonds formed with Glu166, Pro168, and Thr190 contributed significantly to the interaction of M^{pro} with (E,E)-farnesol. The bond formations by residues Asn142 (hydrogen bond), Cys145 and His163 (hydrophobic bond) were responsible for the interaction of rosenonolactone with M^{pro}. Further, considering the cyperusol B1 compound, hydrogen bonds by His41 and His164 along with hydrophobic bonds by His41, Met49, and Cys145 residues contributed to its interaction with M^{pro}. Finally, the interaction of adenosine with M^{pro} was mediated by hydrogen bond formation involving Asn142, Phe140, and Glu166 residues and hydrophobic bonds involving Cys145 residue. Most phytochemicals have exhibited similar binding interactions at the active pocket of M^{pro} in comparison with

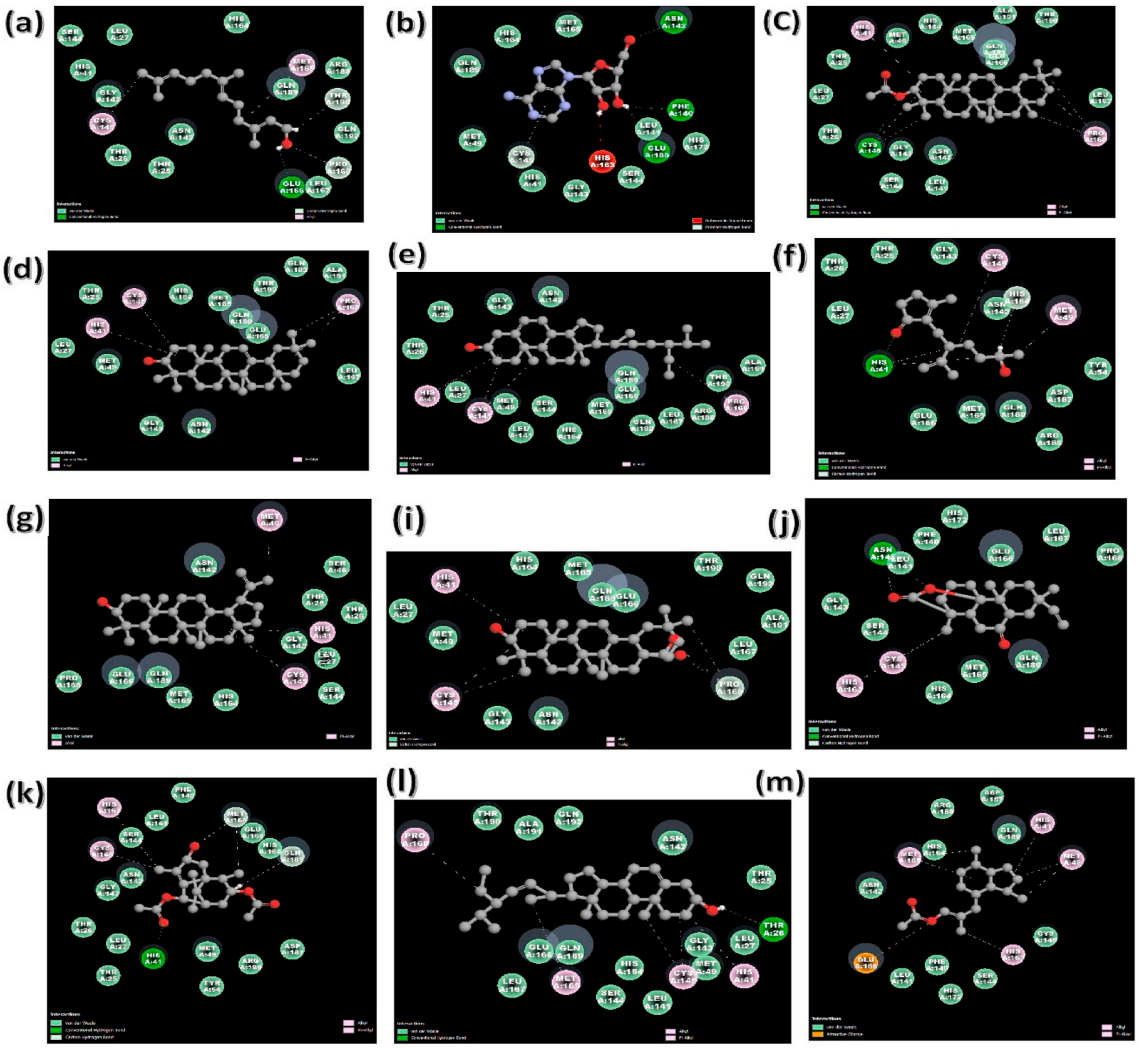

Fig. 1. Molecular interactions between M^{pro} and the 12 identified ligands: (a) (E,E)-farnesol, (b) adenosine, (c) β-amyrin, (d) β-amyrin acetate, (e) β-sitosterol, (f) cyperusol, (g) lupeol, (i) oleanolic acid, (j) rosenanolactone, (k) sugetriol-3,9-diacetate, (l) stigmasta-5,22-dien-3-ol, (m) valerenyl acetate.

standard drugs such as lopinavir and ritonavir.

3.4. Interaction pharmacophore analysis

The comparative analysis of receptor–ligand interactions showed potential ligands to target SARS-CoV-2 M^{pro}. Four lead ligands, namely oleanolic acid, β-amyrin, stigmasta-5,22-dien-3-ol and valrenyl acetate were considered as potential phytochemicals based on their interaction and binding affinities. The ligands β-amyrin and oleanolic acid showed a total of four hydrophobic features whereas ligand valrenyl acetate showed a total of five hydrophobic features and one ionic feature. The ligand stigmasta-5,22-dien-3-ol showed a total of two hydrogen features and four hydrophobic features as displayed in Fig. 2.

3.5. Molecular dynamics simulations

3.5.1. Root mean square deviation

To gain a deeper insight into the effects of protein structural changes and flexibility on the complex interaction profile, MD simulations were performed [40]. The RMSD plots of 6LU7 (M^{pro}) complexed with oleanolic acid (OLE), β-amyrin (BET), stigmasta-5,22-dien-3-ol (STI) and valrenyl acetate (VAL) are shown in Fig. 3. RMSD was calculated for protein backbone atoms for all the four complex structures that converged during the 50 ns MD simulation. The average RMSD values were calculated for the entire simulation trajectories. The average values of RMSD for oleanolic acid, β-amyrin, stigmasta-5,22-dien-3-ol, and valrenyl acetate were 0.44, 0.24, 0.27, and 0.34 nm respectively. Such low RMSD values clearly point towards stability of all the four complexes [41]. From this data, it can be further inferred that the complexes 6LU7-BET (M^{pro}–β-amyrin complex) and 6LU7-STI (M^{pro}–-stigmasta-5,22-dien-3-ol complex) were comparatively more stable.

3.5.2. Root mean square fluctuation

The mobility and flexibility of receptor–ligand complex structures are represented by the RMSF value of Cα atoms of the receptor [41]. In all the complexes studied, fluctuations for the amino acid residues corresponding to domains I and II were the lowest whereas, for domain III, it was the highest (shown in Fig. 4). Overall, the fluctuations of various active site amino acid residues (Thr26, Asn142, Phe140, Gly143, His163, Glu166, and His172) [42] were less for 6LU7-BET and 6LU7-STI complexes in comparison with other complexes, as shown in Table 4. Such low fluctuations of these active site residues in the two complexes further suggest that these residues within the active site of M^{pro} interact favourably with ligands [43].

3.5.3. Radius of gyration

The compactness of the system and its change with time is indicated by Rg measurement of a protein backbone [44]. Rg was determined for

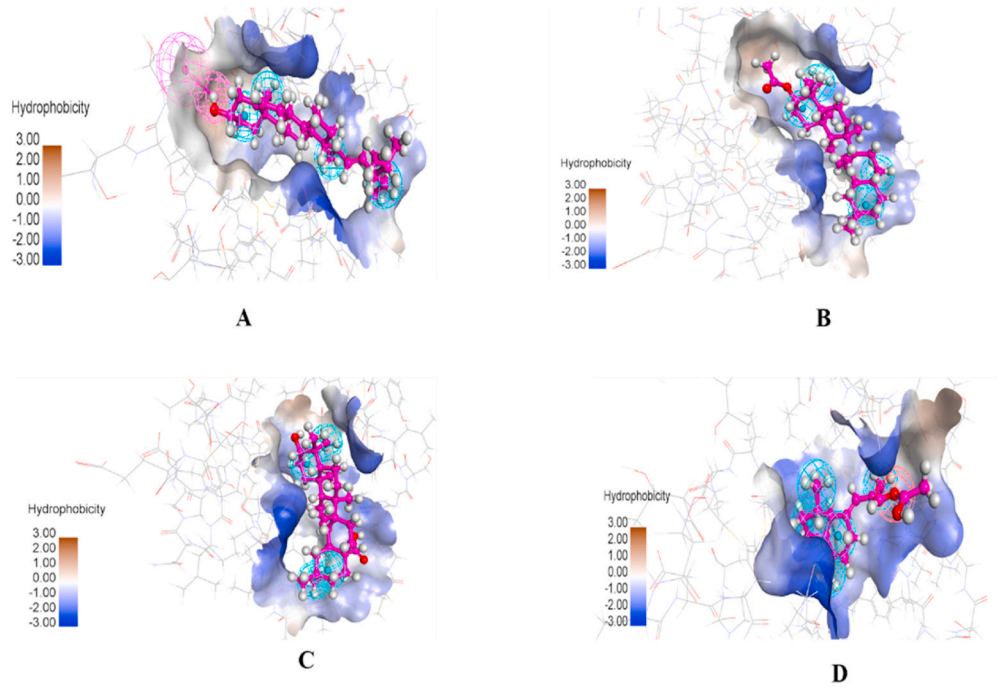

Fig. 2. Generated receptor-ligand pharmacophore models. cyan colour indicates hydrophobic (H) and magenta colour indicates hydrogen bond donor (HBD). A: M^{pro}-stigmasta −5,22-dien-3-ol, B:M^{pro}-β-amyrin, C:M^{pro}-oleanolic acid, D:M^{pro}-valrenyl acetate.

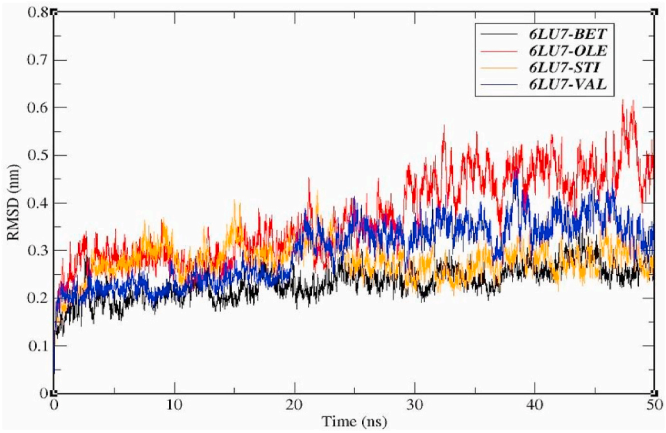

Fig. 3. RMSD study plot of screened protein-ligand complexes for 50 ns MD Simulation of M^{pro}-β-amyrin (Black), M^{pro}-oleanolic acid (Red), M^{pro}-stigmasta −5,22-dien-3-ol (Yellow), M^{pro}-valrenyl acetate (Blue).

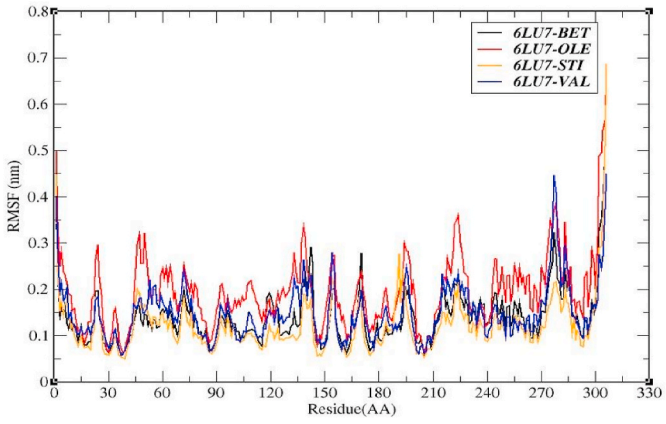

Fig. 4. RMSF study plot of screened protein-ligand complexes for 50 ns MD Simulation of M^{pro}- β-amyrin (Black), M^{pro}-oleanolic acid (Red), M^{pro}-stigmasta −5,22-dien-3-ol (Yellow), M^{pro}-valrenyl acetate (Blue).

each trajectory in the four complexes. The obtained average Rg values for the complexes 6LU7-BET, 6LU7-STI, 6LU7-OLE, and 6LU7-VAL were 2.20, 2.19, 2.23 and 2.2 nm respectively, indicating that the ligands β-amyrin, stigmasta-5,22-dien-3-ol and valrenyl acetate exhibit a rigid nature on binding with M^{pro} (displayed in Fig. 5).

3.5.4. Solvent accessible surface area

The degree of expansion of protein volume in each system was assessed by estimating the average SASA values from individual MD trajectories as shown in Fig. 6 [45]. The SASA values of the four complexes ranged from 149 nm^2 to 152 nm^2. The SASA values corresponding to 6LU7-STI (151.5492 nm^2) and 6LU7-OLE (151.5492 nm^2) were slightly higher than the 6LU7-BET (149.87 nm^2) and 6LU7-VAL (146.47 nm^2) complexes suggesting a slight expansion of M^{pro} during its interaction with stigmasta-5,22-dien-3-ol and oleanolic acid and less expansion upon binding with β-amyrin and valrenyl acetate.

3.6. MM/PBSA: binding free energy calculation

The total binding energy (ΔG_{bind}) of the complex, contributed by various energy terms during MD simulation, were also studied. The MM/PBSA energy values of the top four complexes obtained from GROMACS is presented in Table 5. The complex 6LU7-β-amyrin exhibited the highest binding energy value of −123.942 ± 14.154 kJ/mol followed by 6LU7-stigmasta-5,22-dien-3-ol with an energy value of −121.468 ± 13.078 kJ/mol, indicating stronger interactions between the ligands β-amyrin and stigmasta-5,22-dien-3-ol and SARS-CoV-2 M^{pro}. Additionally, the Van der waal energy exhibited by complexes 6LU7-β-amyrin and 6LU7-stigmasta-5,22-dien-3-ol are −168.875 ± 13.484 kJ/mol and −158.65 ± 13.039 kJ/mol respectively, indicating stronger intermolecular interactions between the ligands and protein thereby strengthening the binding affinity.

Table 4
RMSF value for the active site residues of protein-ligand complexes.

Complexes	Active Site Residues						
	Thr 26	Asn 142	Phe 140	Gly 143	His 163	Glu 166	His 172
	(nm)	(nm)	(nm)	(nm)	(nm)	(nm)	(nm)
6LU7_oleanolic acid (6LU7-OLE)	0.1881	0.2053	0.2404	0.1808	0.1026	0.1662	0.1766
6LU7_β- amyrin (6LU7-BET)	0.117	0.2905	0.2042	0.2598	0.0715	0.1178	0.1197
6LU7_stigmasta-5,22-dien-3-ol (6LU7-STI)	0.1085	0.1789	0.1598	0.1316	0.0582	0.0936	0.0844
6LU7_valrenyl acetate (6LU7-VAL)	0.1251	0.2303	0.1864	0.1838	0.0995	0.115	0.1392

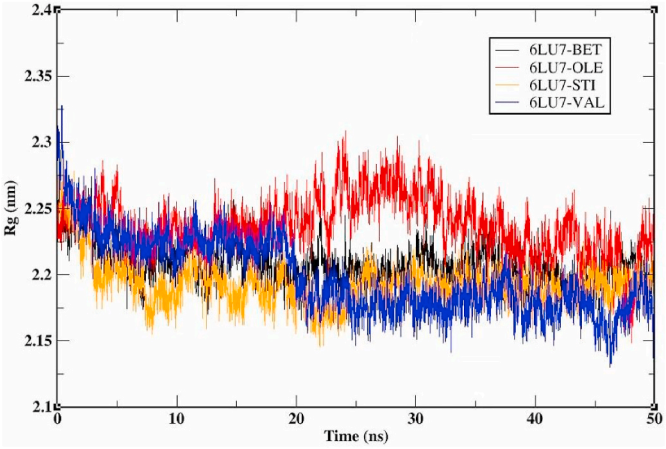

Fig. 5. Rg study plot of screened protein-ligand complexes for 50 ns MD Simulation of M^{pro}- β-amyrin (Black), M^{pro}-oleanolic acid (Red), M^{pro}-stigmasta −5,22-dien-3-ol (Yellow), M^{pro}-valrenyl acetate (Blue).

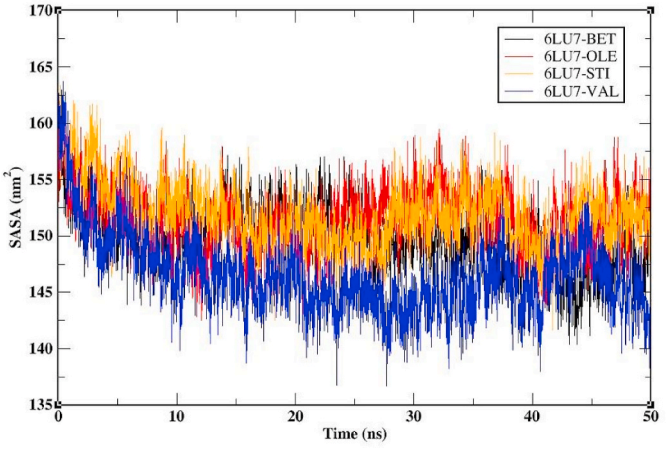

Fig. 6. SASA study plot of screened protein-ligand complexes for 50 ns MD Simulation of M^{pro}-β-amyrin (Black), M^{pro}-oleanolic acid (Red), M^{pro}-stigmasta −5,22-dien-3-ol (Yellow), M^{pro} valrenyl acetate (Blue).

3.7. ADMET studies and biological activity

The MD simulation studies and MM/PBSA calculations showed that β-amyrin and stigmasta-5,22-dien-3-ol exhibit good stability and binding affinity. The pharmacokinetics and toxicity parameters (ADMET) predictions revealed that β-amyrin and stigmasta-5,22-dien-3-ol exhibit logS values of −6.957 and −6.682 respectively, indicating reasonable water solubility. Both the compounds also exhibited admirable oral permeability as observed by their Caco-2 permeability values of 1.286 for β-amyrin and 1.213 for stigmasta-5,22-dien-3-ol. The intestine is generally the primary site for an orally-administered drug. The pkCSM tool predicts % intestinal absorption (human) to represent the absorption of the drug molecule in the human intestine. β-amyrin and stigmasta-5,22-dien-3-ol displayed intestinal absorption of 100% and 94.97% respectively, thereby demonstrating that these compounds are completely absorbed in the intestine.

The steady-state volume of distribution (VDss) is a theoretical value that predicts the total volume of a drug that needs to be uniformly distributed to give the same concentration as blood plasma. A higher VD value (log VDss >0.45) is indicative of high drug distribution in tissues in comparison to plasma. The logarithmic VDss values for β-amyrin and stigmasta-5,22-dien-3-ol were 0.2 and 0.178 respectively. The fraction of unbound drug in plasma is given by the criterion fraction unbound (human). The logarithmic ratio of brain to plasma drug concentration gives blood–brain barrier (BBB) permeability. The value ranges between the upper limit >0.3 to a lower limit < −1, where logBB>0.3 indicates that the drug has good BBB permeability; molecules with logBB < -1 are poorly distributed in the brain. It is a crucial parameter to be considered—to help reduce toxic side effects and improve efficacy of drugs intended to work within the brain. β-amyrin and stigmasta-5,22-dien-3-ol exhibited logBB of 0.661 and 0.771 respectively, indicating that the drugs can readily cross BBB. Similarly, central nervous system (CNS) permeability, measured as logPS, assesses the ability of a drug to penetrate CNS. Compounds with a logPS > -2 are considered to penetrate CNS while those with logPS < −3 do not penetrate CNS. From the pkCSM results, it was observed that β-amyrin and stigmasta-5,22-dien-3-ol have logPS values of −2.077 and −1.652 respectively.

Metabolism of the drug is measured by its ability to inhibit cytochrome P450, an important detoxification enzyme in the body. A compound is considered to be a cytochrome P450 inhibitor if the concentration required for 50% inhibition is less than 10 μM. From the results, it was observed that both β-amyrin and stigmasta-5,22-dien-3-ol are not inhibitors of different isoforms of cytochrome P450 such as CYP1A2, CYP2C19, CYP2C9, CYP2D6, and CYP3A4.

The two important criteria that were considered to determine the

Table 5
MM-PBSA energy values of respective complexes from GROMACS.

Complex	Van der waal energy	Electrostatic energy	Polar solvation energy	SASA energy	Binding energy
	(kJ/mol)	(kJ/mol)	(kJ/mol)	(kJ/mol)	(kJ/mol)
6LU7_ β-amyrin (6LU7-BET)	−168.875 ± 13.484	−3.750 ± 2.821	64.120 ± 10.256	−15.434 ± 1.171	−123.942 ± 14.154
6LU7_oleanolic acid (6LU7-OLE)	−127.053 ± 15.499	−8.044 ± 4.328	58.508 ± 11.541	−12.867 ± 1.907	−89.456 ± 9.823
6LU7_stigmasta-5,22-dien-3-ol (6LU7-STI)	−158.65 ± 13.039	0.323 ± 1.313	52.952 ± 9.929	−16.093 ± 1.942	−121.468 ± 13.078
6LU7_valerenyl acetate (6LU7-VAL)	−87.917 ± 14.410	−38.306 ± 5.710	76.880 ± 7.565	−10.878 ± 1.202	−60.221 ± 10.794

excretion properties of the drug were total clearance (log ml/min/kg) and whether it is a renal organic cation transporter 2 (OCT2) substrate. It was observed that both compounds β-amyrin and stigmasta-5,22-dien-3-ol are not OCT2 substrates. Further, the total drug clearance, given as a combination of hepatic clearance and renal clearance, was found to be −0.134 and 0.618 for β-amyrin and stigmasta-5,22-dien-3-ol respectively.

To assess if the selected compounds have mutagenic potential, the Ames toxicity test was performed in pkCSM tool. A positive Ames result indicates that the compound is toxic and a potential carcinogen. The compounds β-amyrin and stigmasta-5,22-dien-3-ol did not exhibit any Ames toxicity. Further, the acute toxicity of the compounds was measured by considering rat LD50 values. LD50 values for β-amyrin and stigmasta-5,22-dien-3-ol were found to be 2.254 mol/kg and 2.54 mol/kg respectively. Chronic toxicity values were also predicted using oral rat chronic toxicity values. The lowest dose of a compound that results in an observed effect was considered as a benchmark to evaluate the compounds. The predicted log lowest observed adverse effect (LOAEL) was 2.194 and 0.872 for β-amyrin and stigmasta-5,22-dien-3-ol respectively. The lethal concentration values were calculated based on the concentration of drug required to cause the death of 50% flathead minnows. For a given compound, LC50 values below 0.5 mM (log LC50 < -0.3) represent high acute toxicity. The minnow toxicity (log mM) was found to be −2.547 for β-amyrin and −1.657 for stigmasta-5,22-dien-3-ol. Both compounds displayed high acute toxicity. The results for ADMET studies are tabulated in Supplementary Table S4. Overall, the ADMET prediction values indicate that both the compounds are moderately safe and need to be verified experimentally.

The biological activities of β-amyrin and stigmasta-5,22-dien-3-ol were determined using an online version of PASS software (presented in Supplementary Table S5). From the results, it is evident that the hit compounds from *C. rotundus* have various antiviral and antioxidant activities.

Pentacyclic triterpenes such as β-amyrin have shown applicability as antiviral agents against herpes simplex virus (HSV) and influenza A [46–48]. β-amyrin is also known for attenuating the cellular oxidative mechanism; this is responsible for its anti-HBV activity [49]. Apart from being a promising anti-viral compound, β-amyrin also finds use as a broad spectrum analgesic and anti-inflammatory agent and also shows anti-Parkinson's activity [50]. Similarly, the compound stigmasta-5,22-dien-3-ol has shown various remarkable properties including anti-oxidant, antibacterial, anti-inflammatory, anti-arthritic, anti-asthmatic and diuretic activities [51]. Recent *in silico* studies have also identified stigmasta-5,22-dien-3-ol as a potential lead molecule against multiple target proteins of SARS-CoV-2 [52]. Thus, it can be anticipated that phytochemicals from *C. rotundus* have the potential to fight against diseases caused by SARS-CoV-2.

4. Conclusion

The necessity to control the COVID-19 pandemic has led to the development of potential hit compounds that can be used to target the main protease of SARS-CoV-2. In this study, we have performed a virtual screening of phytochemicals from *Cyperus rotundus* Linn towards M^{pro} of SARS-CoV-2, to identify the potential molecules with significant docking scores and stable interactions. Molecular dynamics simulation studies further validated the stability of the protein–ligand complexes. Based on the results, β-amyrin and stigmasta-5,22-dien-3-ol can be used as potential inhibitors of SARS-CoV-2 M^{pro}. From the prediction of ADMET and biological activity, it can be confidently interpreted that the identified compounds β-amyrin and stigmasta-5,22-dien-3-ol are capable of exhibiting antiviral activity. *In vitro* and *in vivo* studies are further required to utilize these phytochemicals for COVID-19 treatment. The present study supports the traditional use of *Cyperus rotundus* Linn medicinal plant in the treatment of viral infections and may be useful in the development of novel and effective therapeutics for COVID-19.

Declaration of competing interest

The authors report no conflicts of interest.

Acknowledgement

The authors thank the management of M. S. Ramaiah Institute of Technology, Bengaluru and M. S. Ramaiah University of Applied Sciences, Bengaluru for providing computational facilities. The authors are grateful for the evaluation license of BIOVIA Discovery Studio provided by Dassault Systèmes to perform this research work.

Appendix A. Supplementary data

Supplementary data to this article can be found online at https://doi.org/10.1016/j.compbiomed.2021.104524.

References

[1] H.M. Wahedi, S. Ahmad, S.W. Abbasi, Stilbene-based natural compounds as promising drug candidates against COVID-19, J. Biomol. Struct. Dyn. (2020) 1–10, https://doi.org/10.1080/07391102.2020.1762743.
[2] V.C.C. Cheng, S.K.P. Lau, P.C.Y. Woo, Y.Y. Kwok, Severe acute respiratory syndrome coronavirus as an agent of emerging and reemerging infection, Clin. Microbiol. Rev. 20 (2007) 660–694, https://doi.org/10.1128/CMR.00023-07.
[3] G. Li, E. De Clercq, Therapeutic options for the 2019 novel coronavirus (2019-nCoV), Nat. Rev. Drug Discov. 19 (2020) 149–150, https://doi.org/10.1038/d41573-020-00016-0.
[4] E. Mahase, Coronavirus covid-19 has killed more people than SARS and MERS combined, despite lower case fatality rate, BMJ 368 (2020) m641, https://doi.org/10.1136/bmj.m641.
[5] Z. Zheng, F. Peng, B. Xu, J. Zhao, H. Liu, J. Peng, Q. Li, C. Jiang, Y. Zhou, S. Liu, C. Ye, P. Zhang, Y. Xing, H. Guo, W. Tang, Risk factors of critical & mortal COVID-19 cases: a systematic literature review and meta-analysis, J. Infect. 81 (2020) e16–e25, https://doi.org/10.1016/j.jinf.2020.04.021.
[6] R.E. Jordan, P. Adab, K.K. Cheng, Covid-19: risk factors for severe disease and death, BMJ 368 (2020), https://doi.org/10.1136/bmj.m1198.
[7] P. Sun, X. Lu, C. Xu, W. Sun, B. Pan, Understanding of COVID-19 based on current evidence, J. Med. Virol. 92 (2020) 548–551, https://doi.org/10.1002/jmv.25722.
[8] J. Gee, P. Marquez, J. Su, G.M. Calvert, R. Liu, T. Myers, N. Nair, S. Martin, T. Clark, L. Markowitz, N. Lindsey, B. Zhang, C. Licata, A. Jazwa, M. Sotir, T. Shimabukuro, First month of COVID-19 vaccine safety monitoring — United States, december 14, 2020–january 13, 2021, MMWR Morb. Mortal. Wkly. Rep. 70 (2021) 283–288, https://doi.org/10.15585/mmwr.mm7008e3.
[9] I. Jones, P. Roy, Sputnik V COVID-19 vaccine candidate appears safe and effective, Lancet 397 (2021) 642–643, https://doi.org/10.1016/S0140-6736(21)00191-4.
[10] S. Bagcchi, The world's largest COVID-19 vaccination campaign, Lancet Infect. Dis. 21 (2021) 323, https://doi.org/10.1016/S1473-3099(21)00081-5.
[11] T.J. Med Sci, S. Sîmsek Yavuz, S. Unal, Turkish journal of medical Sciences antiviral treatment of COVID-19, TURKISH J. Med. Sci. 50 (2020) 611–619, https://doi.org/10.3906/sag-2004-145.
[12] S. Boopathi, A.B. Poma, P. Kolandaivel, Novel 2019 coronavirus structure, mechanism of action, antiviral drug promises and rule out against its treatment, J. Biomol. Struct. Dyn. (2020) 1–10, https://doi.org/10.1080/07391102.2020.1758788.
[13] D.J.E. Opstelten, M.J.B. Raamsman, K. Wolfs, M.C. Horzinek, P.J.M. Rottier, Envelope glycoprotein interactions in coronavirus assembly, J. Cell Biol. 131 (1995) 339–349, https://doi.org/10.1083/jcb.131.2.339.
[14] Z. Wu, J.M. McGoogan, Characteristics of and important lessons from the coronavirus disease 2019 (COVID-19) outbreak in China: summary of a report of 72314 cases from the Chinese center for disease control and prevention, JAMA, J. Am. Med. Assoc. 323 (2020) 1239–1242, https://doi.org/10.1001/jama.2020.2648.
[15] P. Csizmadia, MarvinSketch and MarvinView: molecule applets for the world wide web, in: Proc. 3rd Int. Electron. Conf. Synth. Org. Chem., MDPI, Basel, Switzerland, 1999, p. 1775, https://doi.org/10.3390/ecsoc-3-01775.
[16] D.S.N.B.K. Prasanth, M. Murahari, V. Chandramohan, S.P. Panda, L.R. Atmakuri, C. Guntupalli, In silico identification of potential inhibitors from Cinnamon against main protease and spike glycoprotein of SARS CoV-2, J. Biomol. Struct. Dyn. (2020) 1–15, https://doi.org/10.1080/07391102.2020.1779129, 0.
[17] T. Hou, J. Wang, W. Zhang, X. Xu, ADME evaluation in drug discovery. 6. Can oral biavailability in humans be effectively predicted by simple molecular property-based rules? J. Chem. Inf. Model. 47 (2007) 460–463, https://doi.org/10.1021/ci6003515.
[18] D.F. Veber, S.R. Johnson, H.Y. Cheng, B.R. Smith, K.W. Ward, K.D. Kopple, Molecular properties that influence the oral bioavailability of drug candidates, J. Med. Chem. 45 (2002) 2615–2623, https://doi.org/10.1021/jm020017n.
[19] M.E. Elshakre, M.A. Noamaan, H. Moustafa, H. Butt, Density functional theory, chemical reactivity, pharmacological potential and molecular docking of

dihydrothiouracil-indenopyridopyrimidines with human-DNA topoisomerase II, Int. J. Mol. Sci. 21 (2020) 1–27, https://doi.org/10.3390/ijms21041253.
[20] X. Zhou, S. Yu, J. Su, L. Sun, Computational study on new natural compound inhibitors of pyruvate dehydrogenase kinases, Int. J. Mol. Sci. 17 (2016), https://doi.org/10.3390/ijms17030340.
[21] A. Allouche, Software news and updates gabedit — a graphical user interface for computational chemistry softwares, J. Comput. Chem. 32 (2012) 174–182, https://doi.org/10.1002/jcc.
[22] S.T. Baby, S. Sharma, S. Enaganti, R.P. Cherian, Molecular docking and pharmacophore studies of heterocyclic compounds as Heat shock protein 90 (Hsp90) Inhibitors, Bioinformation 12 (2016) 149–155, https://doi.org/10.6026/97320630012149.
[23] U.N. Rafiqi, I. Gul, M. Saifi, N. Nasrullah, J. Ahmad, P. Dash, M. Zainul Abdin, Cloning, identification, and in silico analysis of terpene synthases involved in the competing pathway of artemisinin biosynthesis pathway in Artemisia annua L, Pharmacogn, What Mag. 15 (2019) S38–S46, https://doi.org/10.4103/pm.pm.
[24] N.A. Al-Shar'i, E.K. Al-Rousan, L.I. Fakhouri, Q.A. Al-Balas, M.A. Hassan, Discovery of a nanomolar glyoxalase-I inhibitor using integrated ligand-based pharmacophore modeling and molecular docking, Med. Chem. Res. 29 (2020) 356–376, https://doi.org/10.1007/s00044-019-02486-3.
[25] M.S. Lee, M. Feig, F.R. Salsbury, C.L. Brooks, New analytic approximation to the standard molecular volume definition and its application to generalized born calculations, J. Comput. Chem. 24 (2003) 1348–1356, https://doi.org/10.1002/jcc.10272.
[26] H. Meduru, Y.T. Wang, J.J.P. Tsai, Y.C. Chen, Finding a potential dipeptidyl peptidase-4 (DPP-4) inhibitor for type-2 diabetes treatment based on molecular docking, pharmacophore generation, and molecular dynamics simulation, Int. J. Mol. Sci. 17 (2016), https://doi.org/10.3390/ijms17060920.
[27] E. Lindahl, M.J. Abraham, H. Berk, D. Van Der Spoel, GROMACS 2019.4 Manual, GROMACS Doc, 2019.
[28] B.S. Gangadharappa, R. Sharath, P.D. Revanasiddappa, V. Chandramohan, M. Balasubramaniam, T.P. Vardhineni, Structural insights of metallo-beta-lactamase revealed an effective way of inhibition of enzyme by natural inhibitors, J. Biomol. Struct. Dyn. 38 (2020) 3757–3771, https://doi.org/10.1080/07391102.2019.1667265.
[29] B. Kumar, P. Parasuraman, T.P.K. Murthy, M. Murahari, V. Chandramohan, In silico screening of therapeutic potentials from Strychnos nux-vomica against the dimeric main protease (Mpro) structure of SARS-CoV-2, J. Biomol. Struct. Dyn. (2021) 1–19.
[30] S. Krishna, S.B. Kumar, T.P.K. Murthy, M. Murahari, Structure-based design approach of potential Bcl-2 inhibitors for cancer chemotherapy, Comput. Biol. Med. (2021), 104455.
[31] A.W. Schüttelkopf, D.M.F. Van Aalten, PRODRG: a tool for high-throughput crystallography of protein-ligand complexes, Acta Crystallogr. Sect. D Biol. Crystallogr. 60 (2004) 1355–1363, https://doi.org/10.1107/S0907444904011679.
[32] M. Thangavel, V. Chandramohan, L.H. Shankaraiah, R.L. Jayaraj, K. Poomani, S. Magudeeswaran, H. Govindasamy, R. Vijayakumar, B. Rangasamy, M. Dharmar, E. Namasivayam, Design and molecular dynamic investigations of 7,8-dihydroxy-flavone derivatives as potential neuroprotective agents against alpha-synuclein, Sci. Rep. 10 (2020) 1–10, https://doi.org/10.1038/s41598-020-57417-9.
[33] R. Kumari, R. Kumar, A. Lynn, G-mmpbsa -A GROMACS tool for high-throughput MM-PBSA calculations, J. Chem. Inf. Model. 54 (2014) 1951–1962, https://doi.org/10.1021/ci500020m.
[34] D.E.V. Pires, T.L. Blundell, D.B. Ascher, pkCSM: predicting small-molecule pharmacokinetic and toxicity properties using graph-based signatures, J. Med. Chem. 58 (2015) 4066–4072, https://doi.org/10.1021/acs.jmedchem.5b00104.
[35] B. Shah, P. Modi, S.R. Sagar, In silico studies on therapeutic agents for COVID-19: drug repurposing approach, Life Sci. 252 (2020), 117652, https://doi.org/10.1016/j.lfs.2020.117652.
[36] J. Fei, L. Zhou, T. Liu, X.Y. Tang, Pharmacophore modeling, virtual screening, and mo-lecular docking studies for discovery of novel Akt2 inhibitors, Int. J. Med. Sci. 10 (2013) 265–275, https://doi.org/10.7150/ijms.5344.
[37] J.K. Gagnon, S.M. Law, C.L. Brooks, Flexible CDOCKER: development and application of a pseudo-explicit structure-based docking method within CHARMM, J. Comput. Chem. 37 (2016) 753–762, https://doi.org/10.1002/jcc.24259.
[38] Y. Fu, Y.N. Sun, K.H. Yi, M.Q. Li, H.F. Cao, J.Z. Li, F. Ye, 3D pharmacophore-based virtual screening and docking approaches toward the discovery of novel HPPD inhibitors, Molecules 22 (2017), https://doi.org/10.3390/molecules22060959.
[39] S. Genheden, U. Ryde, The MM/PBSA and MM/GBSA methods to estimate ligand-binding affinities, Expet Opin. Drug Discov. 10 (2015) 449–461, https://doi.org/10.1517/17460441.2015.1032936.
[40] S. Aliebrahimi, S. Montasser Kouhsari, S.N. Ostad, S.S. Arab, L. Karami, Identification of phytochemicals targeting c-met kinase domain using consensus docking and molecular dynamics simulation studies, Cell Biochem. Biophys. 76 (2018) 135–145, https://doi.org/10.1007/s12013-017-0821-6.
[41] R. Ghosh, A. Chakraborty, A. Biswas, S. Chowdhuri, Evaluation of green tea polyphenols as novel corona virus (SARS CoV-2) main protease (Mpro) inhibitors–an in silico docking and molecular dynamics simulation study, J. Biomol. Struct. Dyn. (2020) 1–13, https://doi.org/10.1080/07391102.2020.1779818.
[42] M. ÖZDEMİR, B. Köksoy, D. Ceyhan, M. Bulut, B. YALCİN, In silico, 6LU7 protein inhibition using dihydroxy-3-phenyl coumarin derivatives for SARS-CoV-2, J. Turkish Chem. Soc. Sect. A Chem. 7 (2020) 691–712, https://doi.org/10.18596/jotcsa.753157.
[43] P. Das, R. Majumder, M. Mandal, P. Basak, In-Silico approach for identification of effective and stable inhibitors for COVID-19 main protease (Mpro) from flavonoid based phytochemical constituents of Calendula officinalis, J. Biomol. Struct. Dyn. (2020) 1–16, https://doi.org/10.1080/07391102.2020.1796799, 0.
[44] P. Chowdhury, In silico investigation of phytoconstituents from Indian medicinal herb 'Tinospora cordifolia (giloy)' against SARS-CoV-2 (COVID-19) by molecular dynamics approach, J. Biomol. Struct. Dyn. (2020) 1–18, https://doi.org/10.1080/07391102.2020.1803968, 0.
[45] S. Alcaro, A. Artese, G. Costa, S. Distinto, F. Ortuso, L. Parrotta, Conformational studies and solvent-accessible surface area analysis of known selective DNA G-Quadruplex binders, Biochimie 93 (2011) 1267–1274, https://doi.org/10.1016/j.biochi.2011.06.014.
[46] G. Rao, J. Sinsheimer, U.K.C.-J. of P. Sciences, Antiviral activity of triterpenoid saponins containing acylated β-amyrin aglycones, J. Pharm. Sci. 63 (1974) 471–473, https://doi.org/10.1002/jps.2600630341, 1974.
[47] M. Heidary Navid, M.N. Laszczyk-Lauer, J. Reichling, P. Schnitzler, Pentacyclic triterpenes in birch bark extract inhibit early step of herpes simplex virus type 1 replication, Phytomedicine 21 (2014) 1273–1280, https://doi.org/10.1016/j.phymed.2014.06.007.
[48] N. Joycharat, H. Greger, O. Hofer, E.S.Phytochemistry, U, Flavaglines and triterpenoids from the leaves of Aglaia forbesii, Phytochemistry 69 (2008) 206–211, 2008.
[49] M.K. Parvez, P. Alam, A.H. Arbab, M.S. Al-Dosari, T.A. Alhowiriny, S.I. Alqasoumi, Analysis of antioxidative and antiviral biomarkers β-amyrin, β-sitosterol, lupeol, ursolic acid in Guiera senegalensis leaves extract by validated HPTLC methods, Saudi Pharmaceut. J. 26 (2018) 685–693, https://doi.org/10.1016/j.jsps.2018.02.022.
[50] C.C. Wei, C.H. Chang, V.H.C. Liao, Anti-Parkinsonian effects of β-amyrin are regulated via LGG-1 involved autophagy pathway in Caenorhabditis elegans, Phytomedicine 36 (2017) 118–125, https://doi.org/10.1016/j.phymed.2017.09.002.
[51] F. Mujeeb, P. Bajpai, N. Pathak, Phytochemical evaluation, antimicrobial activity, and determination of bioactive components from leaves of aegle marmelos, BioMed Res. Int. 2014 (2014), https://doi.org/10.1155/2014/497606.
[52] K. Swaminathan, K.N. Karunakaran, J. Priya Manoharan, S. Vidyalakshmi, SARS-CoV2 multiple target inhibitors from Andrographis Paniculata: an in-silico report Short title: SARS-CoV2 inhibitors from A.Paniculata, Eur. J. Mol. Clin. Med. (2021) 1653–1685, 08.